Phys Chem Minerals (2013) 40:587–595
DOI 10.1007/s00269-013-0595-3

ORIGINAL PAPER

Structural changes in the $FeAl_2O_4$–$FeCr_2O_4$ solid solution series and their consequences on natural Cr-bearing spinels

Davide Lenaz · Henrik Skogby

Received: 23 January 2013 / Accepted: 21 April 2013 / Published online: 8 May 2013

Abstract The influence of Al–Cr substitution on the spinel structure was studied in synthetic single crystals belonging to the $FeCr_2O_4$–$FeAl_2O_4$ series produced by flux growth at 1,000–1,300 °C in controlled atmosphere. Samples were characterized by single-crystal X-ray diffraction, electron microprobe analyses and Mössbauer spectroscopy. Crystals of sufficient size and quality for single-crystal X-ray diffraction were obtained in the ranges $Chr_{0–0.45}$ and $Chr_{70–100}$ but not for intermediate compositions, possibly due to a reduced stability in this range. The increase in chromite component leads to an increase in the cell edge from 8.1534 (6) to 8.3672 (1) Å and a decrease in the *u* parameter from 0.2645 (2) to 0.2628 (1). Chemical analyses show that Fe^{2+} is very close to 1 apfu (0.994–1.007), Al is in the range 0.0793–1.981 apfu, Cr between 0 and 1.925 apfu. In some cases, Fe^{3+} is present in amounts up to 0.031 apfu. Spinels with intermediate Cr content (Chr component between 40 and 60) are strongly zoned with Cr-rich cores and Cr-poor rims. Mössbauer analyses on powdered spinels of the runs from which single crystal has been used for X-ray structural data show values of Fe^{3+}/Fe_{tot} consistently larger than that calculated by EMPA on single crystals, presumably due to chemical variation between single crystals from the same runs. The synthesis runs ended at a temperature of 1,000 °C, but it is possible that cation ordering continued in the Cr-poor samples towards lower temperatures, possibly down to 700 °C.

D. Lenaz (✉)
Department of Mathematics and Geosciences, via Weiss 8, 34127 Trieste, Italy
e-mail: lenaz@units.it

H. Skogby
Department of Geosciences, Swedish Museum of Natural History, 10405 Stockholm, Sweden

Keywords $FeCr_2O_4$–$FeAl_2O_4$ spinel series · Flux-growth synthesis · Single-crystal X-ray diffraction · Mössbauer spectroscopy · Inversion degree

Introduction

The principal constituents of natural chrome spinels are Cr, Al, Mg and Fe^{2+}. During fractional crystallization or partial melting, Cr, Mg and Al behave differently; Cr and Mg are strongly partitioned into the solid, whereas Al is strongly partitioned into the melt (Cookenboo et al. 1997; Lenaz et al. 2000; Barnes and Roeder 2001; Kamenetsky et al. 2001). Partitioning of Mg and Fe^{2+} between spinel, silicate melts and other minerals is strongly temperature-dependent. Moreover, the oxidation state of iron is related to the oxygen fugacity. Given that many studies devoted to the structure of Cr-bearing spinels by single-crystal X-ray diffraction have been performed by several authors. In fact, in the past 25 years, studies of Cr-bearing spinels from mantle xenoliths (Della Giusta et al. 1986; Princivalle et al. 1989; Carraro 2003; Uchida et al. 2005; Nédli et al. 2008) and Alpine peridotites (Basso et al. 1984; Lenaz et al. 2010) that are Al-rich, as well as from ophiolites (Bosi et al. 2004; Derbyshire et al. 2013), layered ultramafic intrusions (Lenaz et al. 2007, 2011, 2012), komatiites (Lenaz et al. 2004a) and kimberlites (Lenaz et al. 2009; Lenaz et al. submitted) that are Cr-rich have been published in order to better characterize these spinels and yield new contributions to their genesis (tectonic setting and oxygen fugacity) and cooling history.

As evident from the studies listed above, the $FeAl_2O_4$ and $FeCr_2O_4$ end-members are very common and important components of spinel solid solutions in several geological environments. Due to the chemical complexity frequently observed in natural spinels and the difficulties in

precise site assignment of the major cations, synthetic analogues of well-defined compositions are often studied. Among the Cr-bearing spinels, the $MgCr_2O_4$–$MgFe_2O_4$ (Lenaz et al. 2006; Lenaz and Lughi 2013), $MgCr_2O_4$–$FeCr_2O_4$ (Lenaz et al. 2004b; Lenaz and Lughi 2013) and $MgCr_2O_4$–$MgAl_2O_4$ (Hålenius et al. 2010) solid solutions have been explored during recent years.

The spinel structure is based on a nearly ideal cubic close-packed array of oxygen atoms with tetrahedral (T) and octahedral (M) cavities. One-eighth of the T sites and one-half of the M sites are filled by heterovalent cations A and B in the ratio AB_2O_4, where A = (Mg, Fe^{2+}, Zn and Mn) and B = (Al, Fe^{3+} and Cr^{3+}), in common 2–3 spinels. In general, spinels do not show the ideal configurations, with all A cations exclusively in T sites and all B cations in M sites. Consequently, the crystal-chemistry of spinels may be described by the general formula $^{IV}(A_{1-i}B_i)^{VI}(A_iB_{2-i})O_4$, where "*i*" refers to the so-called inversion parameter. Two ordered configurations are stable at low temperature, one with $i = 0$ (normal spinel; e.g., $MgAl_2O_4$, $FeAl_2O_4$, $MgCr_2O_4$ and $FeCr_2O_4$) and another with $i = 1$ (inverse spinel; e.g., $MgFe_2O_4$ and Fe_3O_4). Disorder occurs at increasing temperature, leading to intersite exchange of the A and B cations over the two sites. Modifications of T–O and M–O bond distances to accommodate various cations and/or cation ordering determine variations in the oxygen positional parameter *u* and the cell edge a (Lavina et al. 2002). For chromium-containing spinels, the large excess octahedral crystal field stabilization energy of Cr^{3+} ($\Delta CFSE_{(oct-tet)} \approx 160$ kJ/mol; O'Neill and Navrotsky 1984) should ensure that Cr-bearing spinels have an almost completely normal cation distribution (Urusov 1983). Consequently, differences in the a and *u* values for the spinels are expected to be related to Al → Cr in M site and $Fe^{2+} \leftrightarrow$ Al substitutions between M and T sites.

Single-crystal X-ray diffraction and electron microprobe analyses were used in this study for crystal chemical characterization of the $FeAl_2O_4$–$FeCr_2O_4$ series. Mössbauer spectroscopy was also utilized to determine the oxidation state of Fe in the studied samples. Both methodologies have been used to characterize the variation in structural parameters over the series and make some considerations about their behaviour in comparison with natural analogues.

Experimental

Crystal growth

Single crystals along the hercynite–chromite join were synthesized using a flux-growth method. Analytical grade $Al(OH)_3$, Cr_2O_3 and Fe_2O_3 powders were dehydrated and dried before mixing with $Na_2B_4O_7$, used as flux compound. Around 6 g of starting material was ground under acetone in an agate mortar and mixed with flux/nutrient ratios ranging from 1.9 to 3.2 depending on composition. The mixture was loaded in a 12 mL yttria-stabilized Pt/Au (5 %) crucible and covered by a lid. A vertical tube furnace equipped with programmable temperature controller, and controlled atmosphere flow system was used. In order to obtain a homogeneous melt, the load was heated at 1,300 °C for 24 h. Subsequently, the temperature was linearly decreased by 300 °C with a cooling rate of 4 °C h^{-1}. A reducing atmosphere was provided by a continuous flow of high-purity CO_2 and H_2 gases through the furnace. The CO_2:H_2 ratio was maintained by TYLAN flow controllers and was kept constant at 1:1, resulting in an oxygen fugacity ranging from 10^{-11} to 10^{-16} bars from 1,300 to 1,000 °C. The thermal runs were ended turning off the furnace, and the product was allowed to cool more rapidly to room temperature (below 500 °C within 2 h). Successful runs consisted of spinel and borate crystals dispersed in borate glass, which was dissolved in warm diluted HCl. Experimental problems were encountered for intermediate starting compositions which frequently resulted in only borates as crystalline products, strongly zoned spinel crystals, or crystals of insufficient size.

Single-crystal X-ray diffraction and microprobe analyses

X-ray diffraction data of the synthetic spinels were recorded on an automated KUMA-KM4 (K-geometry) diffractometer, using MoKα radiation, monochromatized by a flat graphite crystal. Data collection was made, according to Della Giusta et al. (1996), up to 55° of θ in the ω−2θ scan mode, scan width 1.8° 2θ, counting time from 20 to 50 s, depending on peak standard deviation. Twenty-four equivalent reflections of (12 8 4) (about 80° of 2θ), or (8 4 0) (at about 40° of 2θ) in the case of smaller spinels, were accurately centred at both sides of 2θ, and the α_1 peak barycentre was used for cell parameter determination.

Structural refinement using the SHELX-97 programme (Sheldrick 2008) was carried out against Fo^2_{hkl} in the *Fd*–3 *m* space group (with origin at –3 *m*), since no evidence of different symmetry appeared. Refined parameters were the scale factor, oxygen positional parameter (*u*), tetrahedral and octahedral site occupancies and atomic displacement parameters (*U*). Scattering factors were taken from Prince (2004) and Tokonami (1965). The neutral scattering curves, Al versus Fe in the tetrahedral (T) site and Cr versus Al in octahedral (M) site, were assigned to sites involved in isomorphous replacements, with the constraints of full site occupancy. Best refinement results have been obtained by using oxygen in a partly ionized state (70 %). No constraints were imposed by chemical analyses. The crystallographic data are presented in Table 1.

Table 1 Results of structure refinement

Sample	FAC03A	FAC03B	FAC10H Zoned	FAC10H Zoned	FAC10H Zoned	FAC10H Zoned	FAC10E Zoned	FAC10E Zoned	FAC05C Zoned	FAC05C Zoned	FAC05C Zoned	FAC10D	FAC20D
a_0	8.1551 (3)	8.1534 (6)	8.1539 (3)				8.3264 (6)		8.3364 (3)			8.3553 (2)	8.3672 (1)
u	0.2645 (2)	0.2642 (1)	0.2644 (2)				0.2633 (1)		0.2631 (1)			0.2629 (1)	0.2628 (1)
T–O	1.970 (1)	1.966 (2)	1.968 (2)				1.995 (2)		1.993 (2)			1.996 (2)	1.997 (1)
M–O	1.928 (1)	1.9294 (8)	1.928 (1)				1.9768 (9)		1.9813 (8)			1.9869 (8)	1.990 (1)
m.a.n.T	24.6 (8)	24.1 (5)	24.5 (9)				26.5 (4)		25.9 (4)			26.1 (5)	26.3 (6)
m.a.n.M	15.3 (4)	15.1 (3)	14.1 (4)				21.2 (2)		21.5 (3)			22.6 (5)	23.7 (6)
U (M)	0.0080 (5)	0.0078 (3)	0.0061 (5)				0.0046 (1)		0.0048 (1)			0.0037 (1)	0.0033 (1)
U (T)	0.0071 (3)	0.0073 (2)	0.0074 (3)				0.0081 (2)		0.0079 (2)			0.0069 (2)	0.0063 (2)
U (O)	0.0092 (7)	0.0099 (4)	0.0098 (7)				0.0067 (4)		0.0076 (3)			0.0058 (3)	0.0043 (3)
N. refl.	103	122	87				108		117			138	149
R_{int}	6.21	6.75	6.41				6.53		4.58			4.96	7.03
R1	3.22	2.36	3.27				2.19		1.70			2.13	2.58
wR2	5.26	3.75	3.62				3.29		2.72			3.65	3.88
GooF	1.221	1.214	1.253				1.130		1.172			1.225	1.314
Diff. peaks	2.46; −1.29	0.97; −0.64	1.77; −1.32				1.32; −1.57		1.20; −0.79			2.15; −1.65	3.41; −1.69
FeO_{tot}		43.0 (3)	41.37 (3)	41.4 (5)	41.2 (4)	40.9 (5)	35.5 (3)	34.87 (21)	34.0 (3)	33.7 (2)	34.42	33.20 (2)	32.4 (2)
Al_2O_3		58.5 (4)	58.0 (3)	57.8 (3)	57.0 (3)	56.06 (7)	11.9 (6)	9.56 (21)	8.43 (8)	7.6 (4)	9.83	4.3 (2)	1.8 (1)
Cr_2O_3			0.4 (1)	1.0 (2)	1.9 (1)	2.8 (2)	54.1 (8)	56.74 (28)	59.0 (4)	59.7 (6)	56.97	63.3 (4)	66.4 (3)
Sum		101.44	99.80	100.22	100.06	99.77	101.49	101.17	101.40	101.06	101.21	100.86	100.55
FeO		41.8 (3)	41.2 (3)	41.3 (5)	41.1 (1)	40.9 (4)	34.5 (3)	33.99 (21)	33.9 (3)	33.6 (2)	34.04	33.1 (2)	
Fe_2O_3		1.3	0.22	0.14	0.11	0.04	1.14	0.98	0.13	0.12	0.42	0.17	
Sum		101.57	99.82	100.23	100.07	99.77	101.60	101.27	101.41	101.07	101.26	100.88	
T site													
Fe^{2+}		0.843 (6)	0.858 (6)				0.980 (13)		0.972 (6)			0.983 (7)	0.992 (9)
Fe^{3+}		0.004 (2)	0.001 (1)				0.008 (7)		0.004 (5)			0.003 (5)	
Al		0.153 (2)	0.142 (2)				0.012 (4)		0.0232 (8)			0.013 (2)	0.008 (2)
M site													
Fe^{2+}		0.160 (3)	0.149 (2)				0.020 (2)		0.023 (1)			0.0115 (7)	0.0019 (4)
Fe^{3+}		0.025 (4)	0.005 (5)				0.023 (11)					0.001 (3)	
Al		1.817 (6)	1.839 (6)				0.475 (22)		0.329 (3)			0.175 (7)	0.071 (7)
Cr			0.009 (3)				1.483 (18)		1.647 (7)			1.811 (7)	1.925 (7)
F(X)		0.22	0.57				0.47		0.34			0.61	0.42

a_0: cell parameter (Å); *u*: oxygen positional parameter; T–O and M–O: tetrahedral and octahedral bond lengths (Å), respectively; m.a.n.T and M: mean atomic number; U(M), U(T), U(O): displacement parameters for M site, T site and O; N. Refl.: number of unique reflections; R1 all (%), wR2 (%), GooF as defined in Sheldrick (2008). Diff.peaks: maximum and minimum residual electron density (± *e*/Å^3). Space Group: Fd−3 m. Origin fixed at –3 m. Z = 8. Reciprocal space range: $-19 \leq h \leq 19$; $0 \leq k \leq 19$; $0 \leq l \leq 19$. F(x): minimization factor which takes into account the mean of the square differences between calculated and observed parameters, divided by their square standard deviations. Estimated standard deviations in brackets

Ten to fifteen spot analyses were performed on the same Cr-spinels used for X-ray data collection, using a CAMECA-CAMEBAX electron microprobe operating at 15 kV and 15 nA. A 20 s counting time was used for both peak and total background. Synthetic oxide standards (FeO, Al_2O_3 and Cr_2O_3) were used. Raw data were reduced by PAP-type correction software provided by CAMECA. The mineral chemical analyses are reported in Table 1. Additional spinel samples not used for X-ray data collection were analysed to constrain the experimental problems.

The cation distribution (Table 1) between the T and M sites was obtained with the method described by Carbonin et al. (1996) and Lavina et al. (2002), in which crystal chemical parameters are calculated as a function of the atomic fractions at the two sites and fitted to the observed parameters. Site atomic fractions were calculated by minimizing the function F(x) (Table 1), which takes into account the mean of the square differences between calculated and observed parameters divided by their squared standard deviations.

Mössbauer spectroscopy

The oxidation state of Fe in the studied samples was determined by Mössbauer spectroscopy, using a conventional spectrometer system operated in constant acceleration mode with a ^{57}Co source in Rh matrix with a nominal activity of 50 mCi. Absorbers were prepared by grinding 2–11 mg of sample material, which was mixed with ca 80 mg acrylic resin (transoptic powder) and then pressed to a disc of 12 mm diameter under moderate heating. Spectra were acquired over 1,024 channels in the velocity range −4.5 to + 4.5 mm/s and calibrated against an α-Fe foil before folding and reduction to 256 channels. A least-squares fitting software (MDA; Jernberg and Sundqvist 1983) was used to analyse the spectra. The spectra could be adequately fitted with four doublets assigned to Fe^{2+} and one doublet assigned to Fe^{3+}, with the exception of sample FAC20D that did not indicate an Fe^{3+} component and was fitted with three Fe^{2+} doublets (Fig. 1). Several studies have shown that the recoil-free fractions for Fe^{2+} and Fe^{3+} are unequal (e.g., De Grave and Van Alboom 1991; Eeckhout and De Grave 2003). The absorption area ratios obtained for the Fe^{2+}, and Fe^{3+} doublets were accordingly corrected for unequal recoil-free fractions based on the data presented in De Grave and Van Alboom (1991) and the composition of the studied samples, using f-values of 0.687 for Fe^{2+} and 0.887 for Fe^{3+}.

Raman mapping

The microprobe analyses showed the presence of zonation in some crystals, which however were difficult to document by electron backscatter observation in SEM. Instead, to characterize the compositional zonations, Raman spectra were acquired using a Renishaw InVia Spectrometer (objective 50 × with 0.75 NA, 1,200 lines/mm grating, 576 pixel CCD detector) equipped with a near-infrared diode laser at 785 nm., delivering 1.5 mW at the sample surface, focused on a spot of approximately 10 μm^2. The exposure time was 10 s per spectrum.

Results

Due to the experimental problems mentioned above, it was not possible to obtain spinel crystals representing the full $FeAl_2O_4$–$FeCr_2O_4$ solid solution series. Crystals of sufficient size and quality for single-crystal X-ray diffraction were restricted to the ranges $Chr_{0–0.45}$ and $Chr_{70–100}$. The reason for the problems to synthesize crystal of good quality for the intermediate compositions is probably related to a reduced spinel stability in this compositional range. Previous studies have established the existence of a miscibility gap in the solid solution between hercynite and chromite at lower temperatures (Sack and Ghiorso 1991; Cremer 1969).

In the present series, the most evident parameters that are strictly related to the Al for Cr substitution are the cell edge, a, and the oxygen positional parameter, *u*. There is a variation from 8.1534 (6) to 8.3672 (1) Å for the cell edge and from 0.2645 (2) to 0.2628 (1) for the *u* values moving from Al- to Cr-rich compositions (Table 1) (Fig. 2).

Other parameters affected by the compositional changes are the T–O (1.966–1.997 Å) and M–O (1.928–1.990 Å) distances, the mean atomic number showing slight variations for the T site (24.1–26.3 electrons) and the displacement parameter for the T site (0.0071–0.0063) but very large differences for the M site (15.1–23.7 electrons), and the displacement parameters (0.0078–0.0033 for the M site and 0.0092–0.0043 for O) (Table 1).

Chemical analyses show that Fe^{2+} is very close to 1 apfu (0.994–1.007), Al is in the range 0.079–1.981 apfu, and Cr between 0 and 1.925 apfu. In some cases, Fe^{3+} is present in amounts ranging between 0 and 0.031 apfu. As seen in Table 1 and in the preliminary Raman map of Fig. 3, that is the result of a principal component analysis performed on an array of 11,700 Raman spectra, collected through an automated XY stage (the blue areas indicate higher Cr content), some of the spinel crystals show a distinct zonation due to Cr–Al substitution (up to 2 wt%). According to the cation distribution, the inversion degree is quite limited with less than 0.16 divalent cations in M site over the compositional series.

Electron microprobe analyses of additional spinels, not used for X-ray crystal structure refinements, showed that they can be organized in three different groups, those with very low Cr (Chr component lower than 3 %), those with

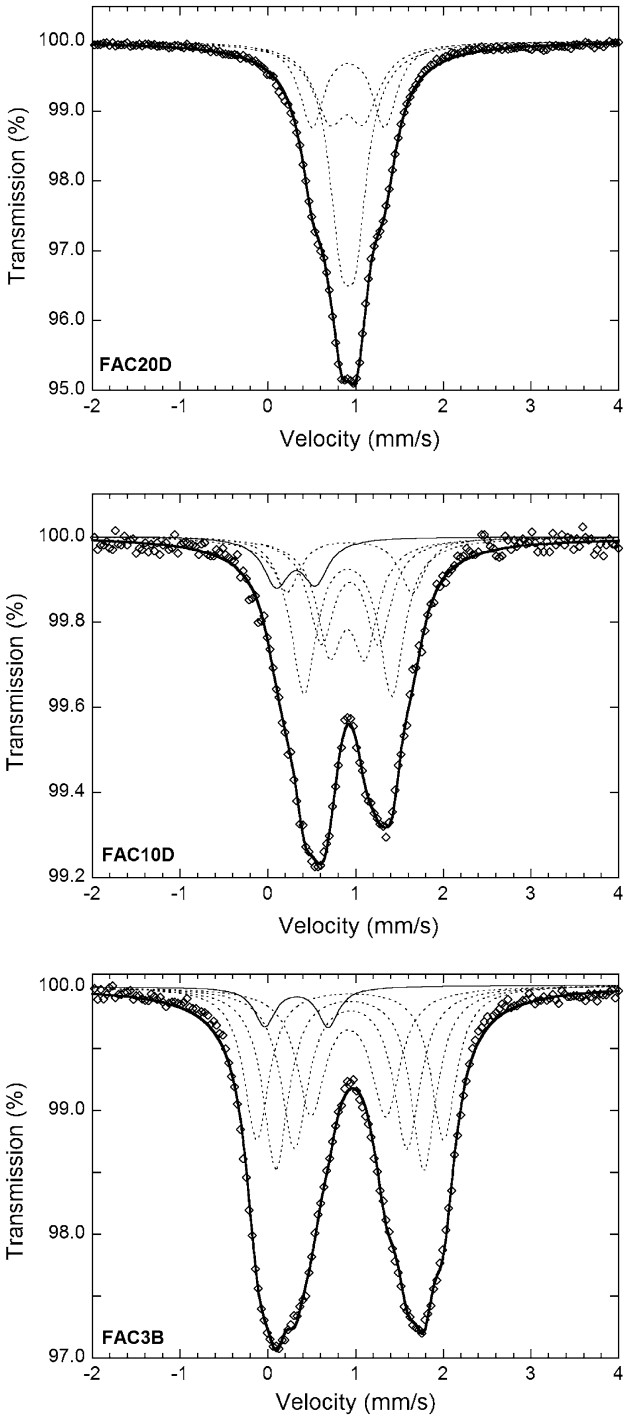

Fig. 1 Representative Mössbauer spectra of spinel samples obtained at room temperature showing varying amounts of Fe^{3+}. *Stippled line* indicates Fe^{2+}, *thin solid lines* indicate Fe^{3+}, and *thick solid line* denotes summed fitted spectrum

very high Cr (Chr component higher than about 65 %) and those with intermediate Cr contents (Chr component of 40–60 %). It is interesting to notice that spinels from the first and the second group are quite homogeneous while those from the third group are strongly zoned with Cr-rich

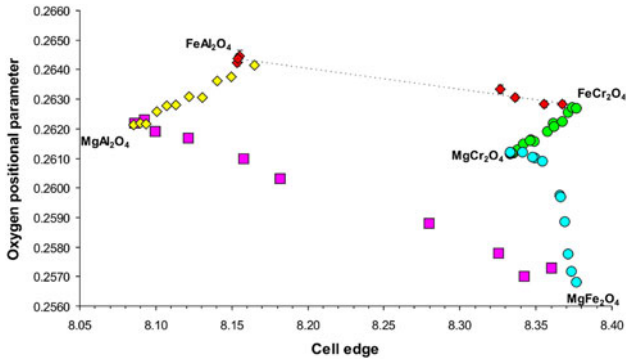

Fig. 2 Oxygen positional parameter, *u*, versus cell edge, a. *Red diamond*: $FeAl_2O_4$–$FeCr_2O_4$ series this study; *yellow square*: $MgAl_2O_4$–$FeAl_2O_4$ (Andreozzi and Lucchesi 2002); *green circle*: $MgCr_2O_4$–$FeCr_2O_4$ series (Lenaz et al. 2004a); *blue circle*: $MgCr_2O_4$–$MgFe_2O_4$ series (Lenaz et al. 2006); *pink square*: $MgAl_2O_4$–$MgFe_2O_4$ series (Nakatsuka et al. 2004)

cores and Cr-poor rims (e.g., sample FAC03b shows $Chr_{2–44}$; sample FAC05a shows $Chr_{1–65}$; sample FAC05e shows $Chr_{1–43}$).

Mössbauer data were obtained on the majority of the synthesized samples. Representative spectra are shown in Fig. 1, and the results from the spectral fitting procedure including hyperfine parameters, absorption areas and oxidation ratios after correction for different Fe^{2+} and Fe^{3+} recoil-free fractions are listed in Table 2. The spectra are dominated by a broad absorption doublet with a centroid shift around 0.92 mm/s considered to be caused by Fe^{2+} both in the T and in the M positions. However, individual doublets cannot be discerned, and the four doublets in the fitting model are not representing distinctive Fe^{2+} environments. The obtained Fe^{3+}/Fe_{tot} ratios show significant variation, ranging from 0 to 8 %. Mössbauer analyses on powdered spinels of the runs from which single crystal has been used for X-ray structural data show values of Fe^{3+}/Fe_{tot} consistently larger than that obtained by EMPA on single crystals (Table 3). A new cation distribution was considered using the Mössbauer data, but the obtained F(x) values are categorically high (Table 4). This discrepancy is presumably due to chemical variation between single crystals from the same runs.

Discussion

The hercynite $FeAl_2O_4$ end-member shows a cell edge of 8.1646 (3) Å and *u* equal to 0.26416 (8) (Andreozzi and Lucchesi 2002), while the cell edge of the chromite $FeCr_2O_4$ end-member is 8.3765 (2) Å and *u* is 0.2627 (1) (Lenaz et al. 2004b). In this study, we found that the most Al-rich samples have lower a values and higher *u* coordinates than that of pure hercynite. The nearly pure hercynite studied by Andreozzi and Lucchesi (2002) is partly

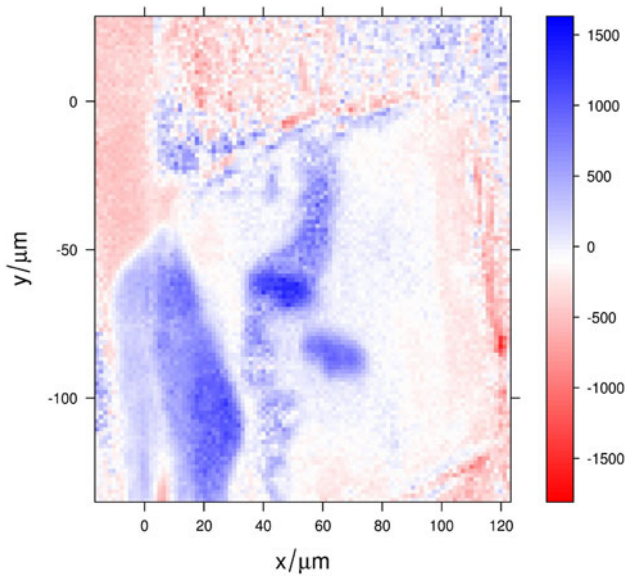

Fig. 3 Raman mapping of crystal FAC05C, differences in color (from *red* to *blue*) indicate an increase in Cr content

inverted, so that the Al and Fe are distributed between M and T sites, it contains also some minor Fe^{3+}, and total Al is lower than 2 cations. The inversion is a common feature related to thermal history, but if we consider a theoretical normal spinel with Fe^{2+} filling only the T site and Al filling the M site, the estimated a should be 8.1409 Å and *u* equal to 0.2668. In this case, the Al-rich spinels studied here fall between the ideal $FeAl_2O_4$ composition and that found by Andreozzi and Lucchesi (2002). This fact could be related to two different causes, the first related to the thermal history and consequently the distribution of Al and Fe between the two sites; however, the thermal conditions are almost the same. The second cause could, possibly, be related to the presence of Cr or Fe^{3+} as observed for the hercynites studied by Andreozzi and Lucchesi (2002). As mentioned before, the octahedral crystal field stabilization energy of Cr^{3+} is very high, and even a limited presence of Cr in the hercynite could prevent a larger inversion degree causing the effects we noticed, as demonstrated in Fig. 4, where the sum of trivalent cation in the T site is plotted against the Cr content. The linear relation is negative and shows a good correlation ($R^2 = 0.98$).

An interesting crystal structural aspect appears in Figs. 5 and 6, where the bond lengths are plotted against the cell edge (T-O in Fig. 5 and M–O in Fig. 6, respectively) for the studied samples, as well as the corresponding values for different natural spinels, including samples from the Alban Hills (Lucchesi et al. 1998), the Somma-Vesuvius (Lucchesi et al. 2010), the metamorphic complex in Fassa Valley (Princivalle et al. 1999), anatectic and metamorphic hercynite (Lavina et al. 2009), Bushveld, Rum and Stillwater layered complexes (Lenaz et al. 2007, 2011, 2012), Ronda and Balmuccia peridotite massifs (Lenaz et al. 2010; Basso et al. 1984), as well as spinels from other occurrences currently under study [iron-bearing spinel

Table 2 Mössbauer parameters obtained for synthetic spinel at room temperature

Sample	FAC03B	FAC05C	FAC10D	FAC10E	FAC20D
Assignment					
Fe^{2+} (1)					
int	22.3	19.0	11.6	17.6	25.0
fwhm	0.34	0.37	0.34	0.36	0.34
cs	0.94	0.91	0.94	0.91	0.92
dq	2.12	1.68	1.42	1.80	0.82
Fe^{2+} (2)					
int	27.2	31.0	33.0	30.3	26.8
fwhm	0.34	0.36	0.34	0.36	0.42
cs	0.94	0.93	0.91	0.93	0.90
dq	1.68	1.19	1.00	1.28	0.38
Fe^{2+} (3)					
int	25.1	22.2	22.3	22.7	48.2
fwhm	0.36	0.33	0.35	0.32	0.32
cs	0.95	0.92	0.94	0.92	0.92
dq	1.28	0.86	0.65	0.92	0.16
Fe^{2+} (4)					
int	20.7	21.2	23.5	21.2	
fwhm	0.39	0.36	0.35	0.36	
cs	0.92	0.93	0.91	0.92	
dq	0.86	0.55	0.40	0.58	
Fe^{3+}					
int	4.7	6.6	9.6	8.2	
fwhm	0.28	0.33	0.35	0.32	
cs	0.33	0.39	0.32	0.38	
dq	0.72	0.39	0.44	0.48	
Fe^{3+}/Fe_{tot}	0.037	0.052	0.076	0.065	0.000

The Fe^{3+}/Fe_{tot} ratios were calculated from the observed intensity relations using recoil-free fractions of 0.687 for Fe^{2+} and 0.887 for Fe^{3+}

Int intensities given in % of total absorption area, *fwhm* full width at half maximum in mm/s, *cs* centroid shift in mm/s, *dq* quadrupole splitting in mm/s

Table 3 Comparison between Fe^{3+}/Fe_{tot} obtained from XRD-EPMA and MS

Sample	Fe^{3+}/Fe_{tot} XRD-EPMA	Fe^{3+}/Fe_{tot} MS
FAC10E	3.0	6.5
FAC05C	0.4	5.2
FAC10D	0.4	7.6

Table 4 New cation distribution according to Fe^{3+}/Fe_{tot} from Mössbauer spectroscopy

Sample	FAC10E[a]	FAC05C[a]	FAC10D
T site			
Fe^{2+}	0.958 (10)	0.972 (10)	0.983 (13)
Fe^{3+}	0.040 (9)	0.002 (3)	0.007 (4)
Al	0.0016 (7)	0.0258 (9)	0.010 (3)
M site			
Fe^{2+}	0.033 (2)	0.022 (2)	0.014 (2)
Fe^{3+}	0.005 (3)	0.021 (10)	0.054 (12)
Al	0.167 (7)	0.322 (3)	0.464 (22)
Cr	1.792 (7)	1.633 (7)	1.467 (18)
Fe^{3+}/Fe_{tot}	4.3	2.3	5.8
F(X)	6.3	3.2	1.4

[a] zoned crystals

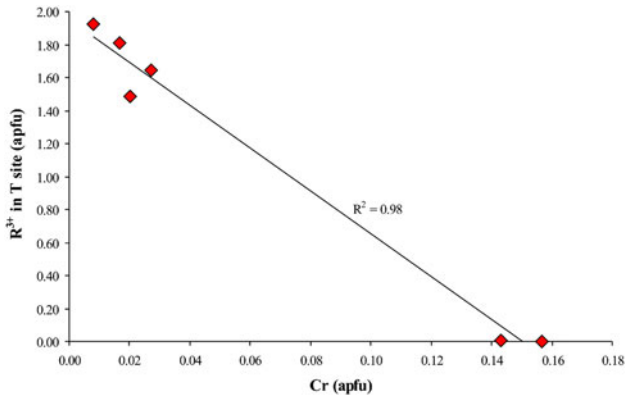

Fig. 4 R^{3+} in T site (Apfu) versus Cr (apfu). *Red diamond*: $FeAl_2O_4$–$FeCr_2O_4$ series this study

from Skye Island (Scotland) and Parker mine (Canada), and Cr-spinels of meteoritic origin and from the Finero peridotitic massif]. The data for the natural samples, R^2 equal to 0.94 and 0.98, respectively, show a trend that parallels the $FeAl_2O_4$–$FeCr_2O_4$ join. Chromites with nearly no Mg are very close to the line connecting the end-members (chromites from meteorites), while spinels with higher Mg content move to lower T–O values due to the minor tetrahedral bond distance of Mg with respect to Fe^{2+} (Lavina et al. 2002).

Spinel *sinsu stricto* and hercynite are normal spinels with a certain degree of inversion. If no inversion is considered, the theoretical cell edges of spinel and hercynite, according to Mg and Fe^{2+} tetrahedral bond lengths and Al octahedral bond length (Lavina et al. 2002), are 8.0935 and 8.1409 Å, respectively (Fig. 7). Two things should be considered in this figure. The first is that the hercynite crystal with no or little Cr content synthesized for this study shows an inversion degree being lower than that of the synthetic hercynite crystals studied by Andreozzi and

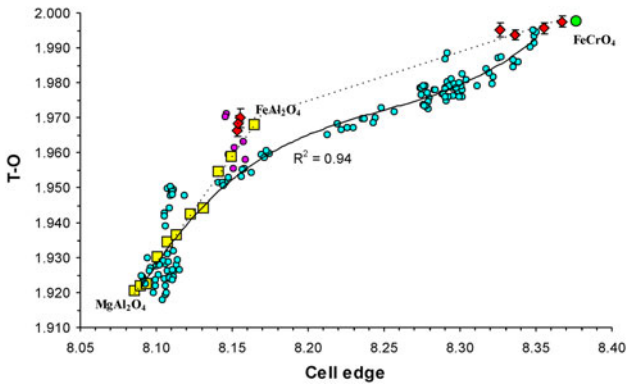

Fig. 5 T-O bond length versus cell edge, **a** *Red diamond*: $FeAl_2O_4$–$FeCr_2O_4$ series this study; *yellow square*: $MgAl_2O_4$–$FeAl_2O_4$ (Andreozzi and Lucchesi 2002); *green circle*: $FeCr_2O_4$ end-member (Lenaz et al. 2004a); *blue circle*: natural Mg–Al–Fe–Cr-spinels (Basso et al. 1984; Lucchesi et al. 1998, 2010; Princivalle et al. 1999; Lenaz et al. 2007, 2010, 2011, 2012); *pink circle*: natural hercynite spinels (Lavina et al. 2009)

Lucchesi (2002), possibly due to the fact that in this run, there was also some chromium possibly influencing the exchange kinetics. Our samples have lower M–O and a values than that of the hercynite by Andreozzi and Lucchesi (2002) that contained 0.09 Fe^{3+} apfu moving towards the theoretical non-inverted $FeAl_2O_4$. The second fact is related to the cooling of the spinels. The here studied Cr-poor hercynite crystals plot in Fig. 7 in the field of natural hercynite crystals studied by Lavina et al. (2009) lying in a position in between the anatectic and the metamorphic spinels. According to those authors, the fast cooled anatectic samples show a range in the calculated value of intracrystalline closure temperature from 700 to 950 °C, while those from the slowly cooled metamorphic rocks have a closure temperature of around 400 °C.

Several studies have experimentally analysed the structural evolution with temperature by means of the variation of oxygen positional parameter *u*, which is strongly influenced by intersite cation exchange and thus correlated with the inversion parameter. Highly ordered natural spinels belonging to the $MgAl_2O_4$–$MgCr_2O_4$ series were studied by means of single-crystal X-ray diffraction using both in situ heating and quenching technique (Carbonin et al. 2002; Martignago et al. 2003; Princivalle et al. 2006). In particular, in three $Mg(Al,Cr)_2O_4$ samples (Carbonin et al. 2002), in which Cr resides only in the octahedral site, *u* parameter variations and hence the order–disorder process started around 700 °C with Cr contents in the Cr samples that affected the occupancy of Al in the tetrahedral site at the highest temperatures. Instead, in a $Mg(Cr, Fe^{3+})_2O_4$ sample (Martignago et al. 2003), this process was triggered at lower temperatures, starting at 550 °C in agreement with the results obtained by Andreozzi et al. (2001) for the synthetic $MgAl_2O_4$–$MgFe_2O_4$

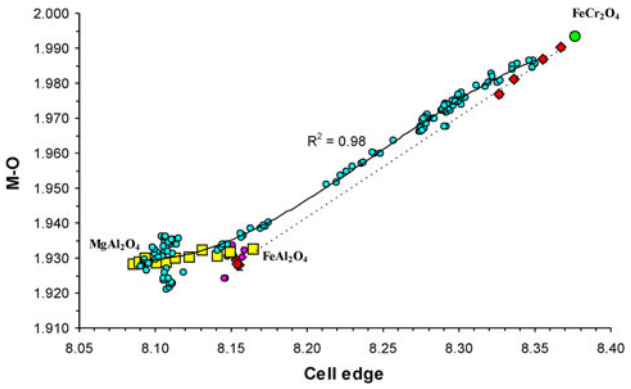

Fig. 6 M–O bond length versus cell edge, **a** *Symbols* as in Fig. 5

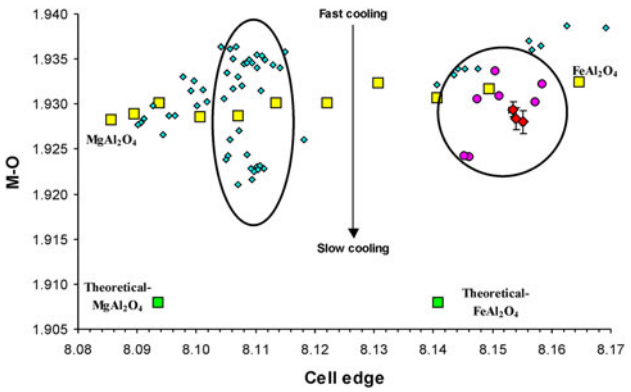

Fig. 7 M–O bond length versus cell edge, **a** *Symbols* as in Fig. 5. *Green square*: theoretical $MgAl_2O_4$ and $FeAl_2O_4$ end-members

series, which showed that Fe^{3+} partitions between T and M sites as a function of both $MgFe_2O_4$ component and temperature. Antao et al. (2005) studied the cation ordering in pure stoichiometric $MgFe_2O_4$ spinel up to 982 °C by in situ synchrotron X-ray powder diffraction. Their results indicated, according to Martignago et al. (2006), that the Mg–Fe^{3+} exchange begins at 581 °C, as revealed by the discontinuity in the cell edge evolution at such temperature. In addition, Princivalle et al. (2012) showed that the time required to reach equilibrium in the ordering processes at 550, 650 and 750 °C for some Mg(Al, Fe^{3+})O_4 spinels is shorter for the high-Fe^{3+} sample than for the low-Fe^{3+} one.

Given the above considerations, even if our synthesis runs ended at a temperature of 1,000 °C, it is likely that cation ordering especially for the Cr-poor samples continued towards lower temperatures despite the faster cooling rate, which could explain the relatively ordered state observed corresponding to equilibration temperatures around 700 °C.

Acknowledgments The Italian C.N.R. financed the installation and maintenance of the microprobe laboratory in Padova. R. Carampin and L. Tauro are kindly acknowledged for technical support. V. Lughi at the Department of Engineering and Architecture (University of Trieste) is acknowledged for the Raman map. Dr. Roman Skála and an anonymous reviewer are thanked for their valuable comments. This work was supported with MURST (PRIN 2010-11) and Trieste University grants.

References

Andreozzi GB, Lucchesi S (2002) Intersite distribution of Fe^{2+} and Mg in the spinel (sensu stricto)-hercynite series by single-crystal X-ray diffraction. Am Mineral 87:1113–1120

Andreozzi GB, Hålenius U, Skogby H (2001) Spectroscopic active $^{IV}Fe^{3+}$–$^{VI}Fe^{3+}$ clusters in spinel-magnesioferrite solid solution crystals: a potential monitor for ordering in oxide spinels. Phys Chem Miner 28:435–444

Antao SM, Hassan I, Parise JB (2005) Cation ordering in magnesioferrite, $MgFe_2O_4$, to 982°C using in situ synchrotron X-ray powder diffraction. Am Mineral 90:219–228

Barnes SJ, Roeder PL (2001) The range of spinel compositions in terrestrial mafic and ultramafic rocks. J Petrol 42:2279–2302

Basso R, Comin-Chiaramonti P, Della Giusta A, Flora O (1984) Crystal chemistry of four Mg-Fe-Al-Cr spinels from the Balmuccia peridotite (Western Italian Alps). N Jb Min Abh 150:1–10

Bosi F, Andreozzi GB, Ferrini V, Lucchesi S (2004) Behavior of cation vacancy in kenotetrahedral Cr-spinels from Albanian eastern belt ophiolites. Am Mineral 89:1367–1373

Carbonin S, Russo U, Della Giusta A (1996) Cation distribution in some natural spinels from X-ray diffraction and Mössbauer spectroscopy. Mineral Mag 60:355–368

Carbonin S, Martignago F, Menegazzo G, Dal Negro A (2002) X-ray single-crystal study of spinels: in situ heating. Phys Chem Miner 29:503–514

Carraro A (2003) Crystal chemistry of chromian spinels from a suite of spinel peridotite mantle xenoliths from the Predazzo Area (Dolomites, Northern Italy). Eur J Miner 15:681–688

Cookenboo HO, Bustin RM, Wilks KR (1997) Detrital chromian spinel compositions used to reconstruct the tectonic setting of provenance: implications for orogeny in the Canadian Cordillera. J Sed Res 67:116–123

Cremer V (1969) Die mischkristallbildung im system chromit-magnetit-hercynit zwischen 1000° and 500°C. N Jb Mineral Abh 111:184–205

De Grave E, Van Alboom A (1991) Evaluation of ferrous and ferric Mössbauer fractions. Phys Chem Mineral 18:337–342

Della Giusta A, Princivalle F, Carbonin S (1986) Crystal chemistry of a suite of natural Cr-bearing spinels with $0.15 < Cr < 1.07$. N Jb Mineral Abh 155:319–330

Della Giusta A, Carbonin S, Ottonello G (1996) Temperature-dependent disorder in a natural Mg–Al–Fe^{2+}–Fe^{3+} spinel. Mineral Mag 60:603–616

Derbyshire EJ, O'Driscoll B, Lenaz D, Gertisser R, Kronz A (2013) Compositional heterogeneity in chromitite seams from the Shetland Ophiolite Complex (Scotland). Lithos 162–163:279–300

Eeckhout SG, De Grave E (2003) Evaluation of ferrous and ferric Mössbauer fractions. Part II. Phys Chem Mineral 30:142–146

Hålenius U, Andreozzi GB, Skogby H (2010) Structural relaxation around Cr^{3+} and the red-green color change in the spinel (sensu stricto)-magnesiochromite ($MgAl_2O_4$–$MgCr_2O_4$) and gahnite–zincochromite ($ZnAl_2O_4$–$ZnCr_2O_4$) solid-solution series. Am Mineral 95:456–462

Jernberg P, Sundqvist T (1983) A versatile Mössbauer analysis program. Uppsala University, Institute of Physics (UUIP-1090)

Kamenetsky V, Crawford AJ, Meffre S (2001) Factors controlling chemistry of magmatic spinel: an empirical study of associated olivine, Cr-spinel and melt inclusions from primitive rocks. J Petrol 42:655–671

Lavina B, Salviulo G, Della Giusta A (2002) Cation distribution and structure modelling of spinel solid solutions. Phys Chem Miner 29:10–18

Lavina B, Cesare B, Álvarez-Valero AM, Uchida H, Downs RT, Koneva A, Dera P (2009) Closure temperatures of intracrystalline ordering in anatectic and metamorphic hercynite, $Fe^{2+}Al_2O_4$. Am Mineral 94:657–665

Lenaz D, Lughi V (2013) Raman study of $MgCr_2O_4$–$Fe^{2+}Cr_2O_4$ and $MgCr_2O_4$–$MgFe_2{}^{3+}O_4$ synthetic series: the effects of Fe^{2+} and Fe^{3+} on Raman shifts. Phys Chem Miner (In press), doi: 10.1007/s00269-013-0586-4

Lenaz D, Kamenetsky V, Crawford AJ, Princivalle F (2000) Melt inclusions in detrital spinel from SE Alps (Italy-Slovenia): a new approach to provenance studies of sedimentary basins. Contrib Mineral Petrol 139:748–758

Lenaz D, Andreozzi GB, Mitra S, Bidyananda M, Princivalle F (2004a) Crystal chemical and ^{57}Fe Mössbauer study of chromite from the Nuggihalli schist belt (India). Mineral Petrol 80:45–57

Lenaz D, Skogby H, Princivalle F, Hålenius U (2004b) Structural changes and valence states in the $MgCr_2O_4$–$FeCr_2O_4$ solid solution series. Phys Chem Miner 31:633–642

Lenaz D, Skogby H, Princivalle F, Hålenius U (2006) The $MgCr_2O_4$–$MgFe_2O_4$ solid solution series: effects of octahedrally coordinated Fe^{3+} on T–O bond lengths. Phys Chem Miner 33:465–474

Lenaz D, Braidotti R, Princivalle F, Garuti G, Zaccarini F (2007) Crystal chemistry and structural refinement of chromites from different chromitite layers and xenoliths of the Bushveld Complex. Eur J Mineral 19:599–609

Lenaz D, Logvinova AM, Princivalle F, Sobolev NV (2009) Structural parameters of chromite included in diamonds and kimberlites from Siberia: a new tool for discriminating ultramafic source. Am Mineral 94:1067–1070

Lenaz D, De Min A, Garuti G, Zaccarini F, Princivalle F (2010) Crystal chemistry of Cr-spinels from the lherzolite mantle peridotite of Ronda (Spain). Am Mineral 95:1323–1328

Lenaz D, O'Driscoll B, Princivalle F (2011) Petrogenesis of the anorthosite–chromitite association: crystal-chemical and petrological insights from the Rum Layered Intrusion, NW Scotland. Contrib Mineral Petrol 162:1201–1213

Lenaz D, Garuti G, Zaccarini F, Cooper RW, Princivalle F (2012) The Stillwater Complex: the response of chromite crystal chemistry to magma injection. Geol Acta 10:33–41

Lenaz D, Skogby H, Logvinova AM, Sobolev NV, Princivalle F (submitted) A micro-Mössbaer study of chromites included in diamond and other mantle-related rocks. Submitted to Phys Chem Miner

Lucchesi S, Amoriello M, Della Giusta A (1998) Crystal chemistry of spinels from xenoliths of the Albian Hills volcanic region. Eur J Mineral 10:473–482

Lucchesi S, Bosi F, Pozzuoli A (2010) Geothermometric study of Mg-rich spinels from the somma-vesuvius volcanic complex (Naples, Italy). Am Mineral 95:617–621

Martignago F, Dal Negro A, Carbonin S (2003) How Cr^{3+} and Fe^{3+} affect Mg–Al order disorder transformation at high temperature in natural spinels. Phys Chem Miner 30:401–408

Martignago F, Andreozzi GB, Dal Negro A (2006) Thermodynamics and kinetics of cation ordering in natural and synthetic Mg(Al, $Fe^{3+})_2O_4$ spinels from in situ high-temperature X-ray diffraction. Am Mineral 91:306–312

Nédli Zs, Princivalle F, Lenaz D, Tóth TM (2008) Crystal chemistry of clinopyroxene and spinel from mantle xenoliths hosted in Late Mesozoic lamprophyres (Villány Mts, S Hungary). N Jb Mineral Abh 185:1–10

O'Neill HStC, Navrotsky A (1984) Cation distributions and thermodynamic properties of binary spinel solid solutions. Am Mineral 69:733–753

Prince E (2004) International Tables for X-ray Crystallography. Volume C: Mathematical, physical and chemical tables, 3rd edn. Sprinter, Dordrecht, The Netherlands

Princivalle F, Della Giusta A, Carbonin S (1989) Comparative crystal chemistry of spinels from some suits of ultramafic rocks. Mineral Petrol 40:117–126

Princivalle F, Della Giusta A, De Min A, Piccirillo EM (1999) Crystal chemistry and significance of cation ordering in Mg–Al rich spinels from high-grade hornfels (Predazzo-Monzoni, NE Italy). Min Mag. 63:257–263

Princivalle F, Martignago F, Dal Negro A (2006) Kinetics of cation ordering in natural Mg(Al, $Cr^{3+})_2O_4$ spinels. Am Mineral 91:313–318

Princivalle F, Martignago F, Nestola F, Dal Negro A (2012) Kinetics of cation ordering in synthetic Mg(Al, $Fe^{3+})_2O_4$ spinels. Eur J Mineral 24:633–643

Sack RO, Ghiorso MS (1991) Chromian spinels as petrogenetic indicators: thermodynamics and petrological applications. Am Mineral 76:827–847

Sheldrick GM (2008) A short history of SHELX. Acta Crystallogr A A64:112–122

Tokonami M (1965) Atomic scattering factor for O^{-2}. Acta Crystallogr A 19:486

Uchida H, Lavina B, Downes RT, Chesley J (2005) Single-crystal X-ray diffraction of spinels from the San Carlos Volcanic Field, Arizona: spinel as a geothermometer. Am Mineral 90:1900–1908

Urusov VS (1983) Interaction of cation on octahedral and tetrahedral sites in simple minerals. Phys Chem Miner 9:1–5